Selective UV Reflecting Mirrors Based on Nanoparticle Multilayers

*J. R. Castro Smirnov, Mauricio E. Calvo, and Hernán Míguez**

A new type of nanostructured selective ultraviolet (UV) reflecting mirror is presented. Periodic porous multilayers with photonic crystal properties are built by spin-coating-assisted layer-by-layer deposition of colloidal suspensions of nanoparticles of ZrO_2 and SiO_2 (electronic band gap at $\lambda < 220$ nm). These optical filters are designed to block well-defined wavelength ranges of the UVA, UVB, and UVC regions of the electromagnetic spectrum while preserving transparency in the visible. The shielding against those spectral regions arises exclusively from optical interference phenomena and depends only on the number of stacked layers and the refractive index contrast between them. In addition, it is shown that the accessible pore network of the as-deposited multilayer allows preparing thin, flexible, self-standing, transferable, and adaptable selective UV filters by polymer infiltration, without significantly losing reflectance intensity, i.e., preserving the dielectric contrast. These films offer a degree of protection comparable to that of traditional ones, without any foreseeable unwanted secondary effects, such as photodegradation, increase of local temperature or, as is the case for organic absorbers, generation of free radicals, all of which are caused by light absorption.

1. Introduction

Research and development of new materials for selectively protecting against UV light has gained a lot of interest due to the increasing number of applications that make use of this radiation in medicine,[1] cosmetics,[2] as well as in a wide range of other industrial processes.[3,4] In general, UV light absorption produces highly reactive free radicals that can induce chemical reactions, resulting in subsequent photodegradation[5,6] and yellowing[7] of polymers, pigments, and dyes. Also, losses of mechanical strength and impact resistance have been reported when polymers are exposed to this sort of radiation.[8] Regarding its effect on human tissue, there is a vast and growing literature reporting harmful effects of ultraviolet radiation on the skin,[9] such as the appearance of cutaneous neoplasm and a variety of photosensitive dermatoses[10] or skin cancer.[11]

J. R. Castro Smirnov, Dr. M. E. Calvo, Dr. H. Míguez
Instituto de Ciencia de Materiales de Sevilla
Consejo Superior de Investigaciones Científicas-Universidad de Sevilla
Américo Vespucio 49, Sevilla, 41092, Spain
E-mail: h.miguez@csic.es

DOI:10. 1002/adfm.201202587

When it comes to protection, completely different approaches are taken depending on the surface to be shielded. In the case of human skin, sun screen lotions containing organic UV absorbers, which typically are compounds containing phenolic groups with intramolecular hydrogen bonds, mixed with TiO_2 or ZnO particles, which contribute to protection with both strong UV light scattering and absorption, are widely spread.[12] In the case of arbitrary material surfaces, both polymeric and sol-gel coatings embedding one of the abovementioned UV blocking compounds are commonly employed.[13] In the last few years, visible transparent materials that merge mechanical flexibility and absorption at certain ultraviolet ranges have been developed by inclusion of the formerly mentioned compounds in polymeric matrices, aiming at creating adaptable coatings for a wide variety of UV sensitive environments.[14–19] However, radical species produced as a consequence of UV light absorption by the organic guest compounds degrade the polymer host, rendering the coating useless after some exposure time.

Alternative approaches to spectrally selective light shielding are based on interference filters, Bragg mirrors, or one dimensional photonic crystals (1DPC).[20,21] One of the most appealing properties of this sort of protection, based on strong reflectance of unwanted frequencies, is that it results from the interference of beams partially reflected and transmitted at the multiple interfaces present in the stack. This mechanism does not involve the generation of excited electronic states thus preventing secondary effects. While it is easy to find a large variety of interference filters in the visible or infrared region, fabrication of absorption-free UV-reflecting dielectric mirrors is a difficult task because there are few materials that can be shaped as thin films with negligible absorption below 300 nm. For this purpose, dense layers of III-nitride semiconductors (III being aluminium, gallium and boron, principally)[22] are stacked in order to achieve light confinement for laser applications in the UV regime. For similar goals, dense SiO_2/ZrO_2 system prepared by plasma sputtering method combined with III-nitrides in microcavities have been used.[23,24] Efficient reflectors for far UV (170–240 nm) have already been realized by single and multiple Fabry-Perot interference filters based on a combination of metal layers, typically aluminium, and dielectrics.[25–27] Polymeric stacks made by dip- or spin-coating are also used to block

UV by optical interference effects but, due to the low refractive index contrast existing between them, from 50 to 100 layers are typically needed to achieve significant reflectance values in a narrow spectral range.[28,29] A recent successful attempt to create an ordered material that reflects selectively UV radiation near 300 nm was based on the structuring of a block copolymer by collective osmotic shock.[30]

Recently, porous 1DPC consisting of SiO_2 and TiO_2 nanoparticles as building blocks were developed[31] and rapidly spread as their applications in different fields were explored.[32] Related to the research discussed here, our group recently proved that these optical structures can be infiltrated with either dissolved polymers[33] or monomers[34] to obtain a hybrid 1DPC that can be lifted off the substrate. Although this is a means to attain highly efficient visible and near infrared mirrors, be they flexible or rigid, their application to the UV range is hindered by the electronic band gap of TiO_2 ($E_g \approx$ 3.2 eV), photonic effects being screened by the strong absorption of TiO_2 at wavelengths below 350 nm.

Herein we present a series of photonic crystal films capable of efficiently blocking different UV wavelength ranges comprised between λ = 200 nm and λ = 400 nm. Our arrangement is based on a porous multilayer structure made by the alternated deposition of layers of ZrO_2 nanocrystals of strictly controlled pore size distribution, which we tailor from the synthesis, and SiO_2 nanoparticles. The large electronic band gaps of the materials employed implies that no optical absorption will prevent the observation of the interference effects sought after. Also, the high refractive index contrast between the different types of nanoparticle layers gives rise to intense Bragg reflections at the targeted wavelengths. In addition, due to the open porosity of the thin layers forming the optical nanostructures, a UV transparent polymer, poly(dimethyl)siloxane (PDMS), could be infiltrated in the structure to yield self-standing, flexible, visibly transparent, transferable, and adaptable highly reflecting filters for UV radiation protection that operate only based on interference effects.

2. Results and Discussion

2.1. Microstructural Characteristics

The goal to attain visibly transparent UV shields based only on interference effects imposed the use of materials that do not present any optical absorption in that range. The choice of SiO_2 and ZrO_2 nanoparticles as building blocks of the multilayers was then mainly determined by their large electronic band gap, which results in lack of optical absorption from the near infrared down to almost λ = 220 nm. While colloidal suspensions of SiO_2 particles had been previously used to make porous mirrors, in general combined with TiO_2 nanocolloids,[31] the preparation of ZrO_2 colloids that could be integrated in an optical quality multilayers by dip- or spin-casting required the modification of already existing sol-gel processing techniques.[35] Peptization in acid medium allows controlling particle size in the desired range, while dialysis provides the necessary surface charge to realize the layer by layer assembly of ZrO_2 particles from methanol/water suspensions. It should be mentioned that particles

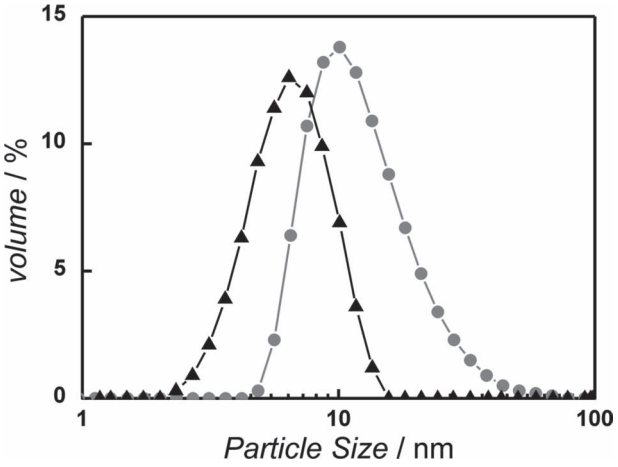

Figure 1. Volumetric particle distribution size of colloidal nanoparticles made of ZrO_2 (black triangles) and SiO_2 (grey circles).

obtained by other ZrO_2 sol-gel synthesis tested were proven to yield poor optical quality multilayers. In **Figure 1** we show the particle size distribution of both types of colloids used in this work. Particle sizes do not exceed the few tens of nanometers (distribution size maxima located at 8 nm and 25 nm for ZrO_2 and SiO_2, respectively). This is a strict requirement to minimize diffuse scattering of both UV and visible light. In addition, size distribution of the particles is narrow enough as to allow the formation of smooth interfaces between the layers of SiO_2 and ZrO_2 in the multilayer.

Field emission scanning electron microscopy (FESEM) images of the cross sections of the multilayers, obtained detecting secondary and backscattered electrons, are shown in **Figure 2**a,b, respectively. Secondary electron image reveals a periodic structure in which the spherical morphology of the bigger SiO_2 particles can be recognized, while the layers made of the smaller ZrO_2 particles appears as an almost continuous layer. A backscattered electron image taken from the same sample region discloses clearly continuous and smooth interfaces between consecutive layers, brighter fringes corresponding to denser ZrO_2 layers. This picture reveals the absence of significant interpenetration that could negatively influence the refractive index contrast and hence the intensity of Bragg reflections from the structure. From these images, we estimate the average thickness of each type of film present in the multilayer, which in this particular case turns out to be around 40 nm for ZrO_2 slabs and 70 nm for SiO_2 ones. FESEM analysis puts in evidence that

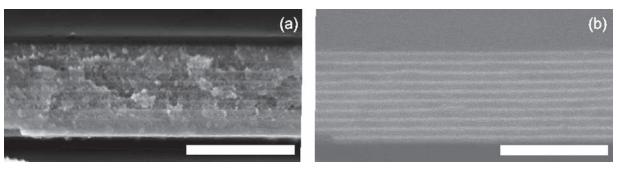

Figure 2. FESEM images of the same region of the cross section of a 20 layer SiO_2/ZrO_2 1DPC deposited onto a silicon substrate, obtained using a) secondary and b) backscattered electron detection. Scale bar is 1 μm in both figures.

up to 20 layers can be stacked by spin coated assisted layer by layer deposition without an intermediate thermal treatment, in general necessary for other combinations of metal oxides.[36] Thus, the particular surface interaction between SiO_2 particles and dialyzed ZrO_2 ones seem to favor the formation of thicker film piles at room temperature, which is in turn convenient for the preparation of flexible films from them (vide infra). It should be mentioned that nanoparticle films are stable against disassembly in the same dispersion medium from which they were deposited.[37] Detailed studies on the mechanical stability of colloidal assemblies propose that particles are likely to be held together by bridges of water hydrogen bonded to the surface, which act as a cement for the structure.[38]

2.2. Optical Properties

2.2.1. One Dimensional Photonic Crystals

Periodic stacking of ZrO_2 and SiO_2 layers gives rise to a modulation of the refractive index in one dimension of the space and, therefore, to its behavior as a one dimensional photonic crystal. A distinct optical feature associated to that periodicity is the presence of a maximum in the reflectance spectra, resulting from the interference of incident light beams partially reflected and transmitted at the interfaces between layers. The method proposed here allows locating this maximum, also referred to as Bragg peak, at different UV wavelength ranges, as illustrated by the series of total reflectance (R_T) spectra plotted in **Figure 3**a. These have been measured from a set of porous ZrO_2/SiO_2 1DPC deposited on a quartz substrate at different final rotation speeds or using different particle concentrations in the precursor suspensions. Complementarily, we measure the total transmittance (T_T) spectra of the coatings, which are shown in Figure 3b. Both families of spectra were acquired using an integrating sphere (see Experimental Section). It is clearly observed that samples can be designed to reflect well-defined spectral ranges in different sub-regions of the ultraviolet spectrum, namely, UVA (from 400 nm to 315 nm), UVB (from 315 nm to 280 nm) and part of UVC (from 280 nm to 100 nm). Significant peak intensity (80%) and width ($\Delta\lambda$ = 50 nm, 0.68 eV) are attained for the number of unit cells (N = 10, a unit cell being defined as a SiO_2/ZrO_2 bilayer) herein stacked as a consequence of the high refractive index contrast between the SiO_2 and ZrO_2 layers. We estimated the absorptance as $A = 1 - R_T - T_T$ (see Figure 3c) to establish the threshold in which optical losses in the multilayer are significant. Most of the samples absorbs near 50% of incident light at λ = 220 nm (5.63 eV), as a consequence of interband absorption in ZrO_2 layers. It can be observed also that, as the position of the Bragg peak shifts to lower wavelength, some overlap with the absorption starts to be significant, which distorts the reflectance and the transmittance spectra for $\lambda <$ 220 nm. The detected fluctuations in absorptance under 3% at longer wavelengths are due to geometrical restrictions to full solid angle light detection in the integrating sphere.[39] This analysis reveals that the UV shield effect, plotted as transmittance in Figure 3b, is totally due to reflection by the film. In addition, the transparency of the samples in the visible region

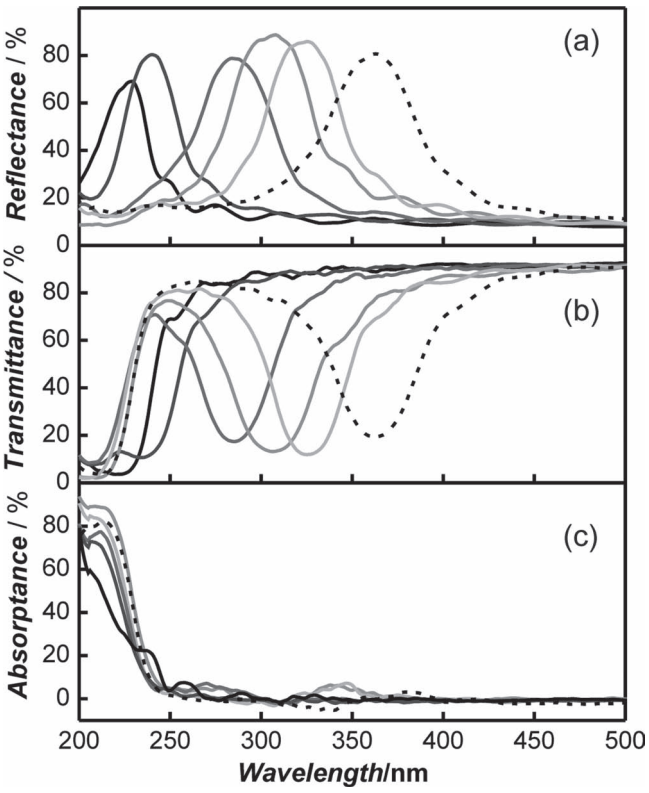

Figure 3. a) Total reflectance, b) total transmittance, and c) absorptance from ZrO_2/SiO_2 interference films. All films were deposited using the same spin coating protocol (ω = 6000 rpm and γ = 11 500 rpm/s) but precursor suspensions with different nanoparticle concentrations (expressed as [SiO_2wt%, ZrO_2wt%]): [1.0, 2.5] (solid black); [1.5, 2.5] (solid grey); [2.0, 2.5] (short dash dark grey); [2.25, 2.5] (solid dark grey); [2.25, 3.0] (solid light grey); and [2.5, 3.0] (short dash black). Unit cell thicknesses were 75 nm, 80 nm, 95 nm, 105 nm, 110 nm, and 125 nm, respectively. Total number of unit cells was 10 in all cases.

(390–750 nm), estimated according to standard methods commonly employed to determine light transmittance of solar radiation for glazing in buildings (ISO 9050:2003), which takes into account the photopic response of the eye, is around 90% in all cases. This is due to the absence of both diffuse scattering, which is a consequence of the strict control over the particle size distribution in the precursor suspensions, and optical absorption. In line or ballistic transmission measurements were also performed and compared to total transmission ones in order to evaluate the amount of light deflected from the incident beam by effect of imperfections in the sample. Results are presented in Figure S1 in the Supporting Information. From them we can conclude that the density of defects has an almost imperceptible effect on the optical response of the coating.

From the fitting of the reflectance spectra we can estimate the refractive indexes, n_i, and the thickness, t, of the constituent layers using a code based on a transfer matrix formalism.[40] Layers' thickness were estimated from SEM images and used as input of the simulations, so that the only free parameters left were the refractive indexes of the individual layers. From this analysis, whose full details can be found in the Supporting Information (Figure S2), we extract $n_{ZrO2} = 1.70$ and $n_{SiO2} = 1.32$,

which implies a pore volume fraction of 50% and 25% respectively. Values of 2.25 and 1.43 are taken for the refractive indexes of bulk ZrO_2 and SiO_2.

2.2.2. 1D Optical Resonators

Another type of photonic structure that can be designed with the formerly described nanoparticle films is an optical porous resonator, which is a multilayer system that presents a disruption of the periodicity, realized in our case by insertion of a thicker mid-layer of SiO_2 beads which will behave as an optical cavity. In terms of photon modes, the consequence of symmetry rupture is the generation of a permitted state at photonic band-gap frequencies, whose track is either a dip spectrally located within the reflectance maximum or the complementary peak in the transmittance minimum. Such features can be readily visualized in Figure S3a,b (Supporting Information). In this sample, the transmission window is designed to be near $\lambda = 310$ nm. This type of systems are capable of blocking a wide region of the UV while still transmitting a narrow range of selected wavelengths and can be useful, for instance, to perform a selective photochemical reaction or polymerization of monomers. They may also be of interest for those phototherapy treatments in which irradiation with narrow UVB ranges, typically centered at $\lambda = 311$ nm, have long been proven as an effective means to treat skin diseases such as psoriasis[41] or vitiligo.[42] From a different perspective, resonant frequencies can be confined in the optical cavity, yielding the enhancement of the interaction between radiation and molecules or nanomateriales located in the cavity.[39] As shown in the previous section, the estimated absorptance ($A = 1 - R_T - T_T$) of the resonator show that all observed optical characteristics are purely due to interference effects.

2.3. Flexible Photonic Structures

2.3.1. Flexible UV Protecting 1DPCs

Since the structures herein presented are porous, they are susceptible to be infiltrated with polymeric compounds to attain a hybrid coating that can eventually be lifted off and behave as a self-standing selective UV protecting film. In this case, we fill the interstitial space with oligomers of PDMS and then trigger the polymerization at a temperature of 110 °C, as described in previous reports.[15,34] A challenge to successfully achieve our goal is the very small average pore size present in ZrO_2 layers, since that could inhibit the diffusion of the oligomers to the deepest layers of the photonic structure. To overcome this obstacle, we infiltrate the structure by spin coating, which forces the deposited liquid phase to enter the voids of the porous multilayer. After that, in order to remove the hybrid film from the substrate, we introduce the sample in liquid nitrogen to reach a temperature below that at which the glass transition of PDMS occurs. Once removed from the Dewar and warmed back to room temperature, the 1DPC can be separated from the substrate. In **Figure 4**a we show reflectance spectra for seven flexible ZrO_2/SiO_2 photonic crystals of different lattice constant. These experiments were made with samples made of 26 layers to reach close to 100% reflectance at 300 nm in the as deposited sample (see Figure S4, Supporting Information). The Bragg peak intensity decreases after PDMS infiltration and lifting off, being then comprised in the range between 60% and 80% in all cases. The decrease in reflectance is due to the lowering of the refractive index contrast between SiO_2 and ZrO_2 layers upon filling of the polymer. These new hybrid polymer/metal oxide samples are mechanically stable and highly flexible, as the images displayed in Figure 4b demonstrate.

2.3.2. Stacks of Hybrid Flexible Films

The mechanical stability and flexibility of films of different lattice constant that shield against well-defined wavelength regions along the 200–400 nm range, as shown in Figure 4, open the way to blocking arbitrarily wide spectral regions by piling them up. In **Figure 5** we show the reflectance spectra of a series of flexible stacks made of an increasing number of multilayers, each one displaying its characteristic Bragg peak at different spectral positions in the UV. Total reflectance, total transmittance and absorptance for stacks containing 1, 3, 5, and 7 films are shown in Figure 5. Films were attached sequentially, starting from the one reflecting the shortest wavelengths up to the one reflecting closer to the blue region. As the number of photonic crystals increases, a wider spectral range is reflected, the entire UVC-UVB-UVA range being efficiently reflected for the case of 7 stacked films while maintaining a transparency of 60% in the visible region. The observed lowering of transparency with respect to a single deposited multilayer is due to the scattering by irregularities in the interfaces between the PDMS layers put in contact, the magnitude of the effect increasing with the number of films in the stack. Since multilayers are embedded in a thick PDMS matrix of smooth but not flat surface, interference effects between the different stacks are not detected in the optical properties of the pile. From the point of view of radiation protection, this simple method can be used to selectively shield against selected spectral regions, as well as to mimic or surpass the effect of a conventional UV absorbing material, as shown in what follows.

2.4. Radiation Protection

The ability of the SiO_2/ZrO_2 flexible photonic crystal films, and stacks of them, to protect from UV light was tested by exposing commercial UV sensitive strips (Control Cure, UV FastCheck Strips, UV process supply Inc.) to the collimated and uniform radiation beam coming out from a solar simulator, employing different combinations of PDMS embedded multilayers to shield them. Detailed analysis of the color changes induced in the strips by effect of the exposure to UV light allows us quantifying the amount of energy they have received from the solar simulator. The performance of the ZrO_2/SiO_2 interference mirrors as UV shields was compared to that of PDMS flexible films, in one case embedding TiO_2 nanoparticles, and, in the other, supporting a thin film of benzophenone-3, a widely employed organic UV absorber, also used in sunscreen lotions.[12] In both cases, UV light blocking occurs only as a consequence of absorption, since the TiO_2 particles employed are too small to give rise to diffuse scattering.

UV sensitive strips were placed below different types of UV protecting films and then illuminated at 1 sun light intensity

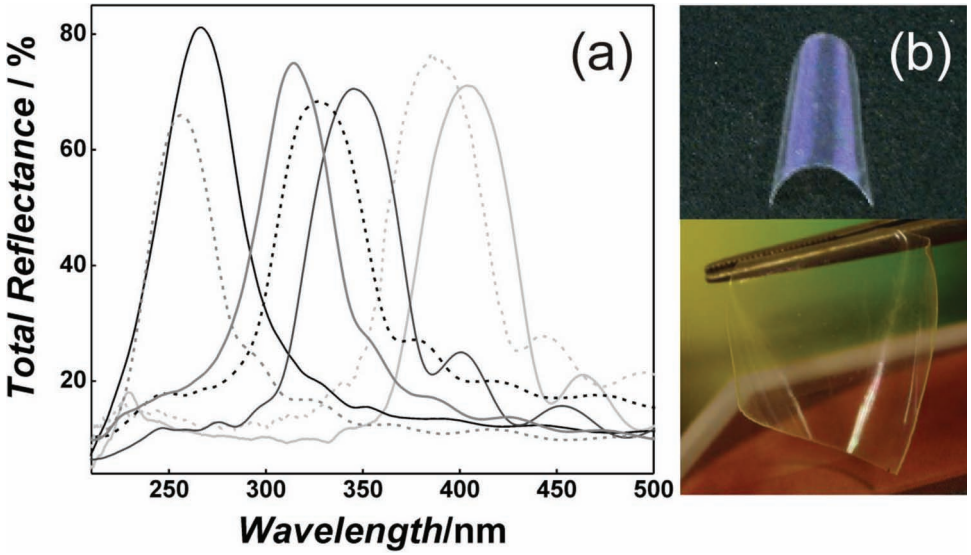

Figure 4. a) Total reflectance spectra of individual flexible hybrid ZrO_2/SiO_2 photonic crystals. Multilayers displaying Bragg reflections from the UV to the visible were prepared using the same spin coating parameters but precursor suspensions with different nanoparticle concentrations (expressed as [SiO_2wt%, ZrO_2wt%]): [1.5, 2.5] (dash grey); [2.0, 2.5] (solid black); [2.25, 2.5] (solid grey); [2.25, 3.0] (dash black); [2.5, 3.0] (grey); [3.0, 2.5] (dash light grey); and [4.0, 2.5] (solid light grey). b) Photographs of hybrid self-standing PDMS/ZrO_2/SiO_2 multilayer films.

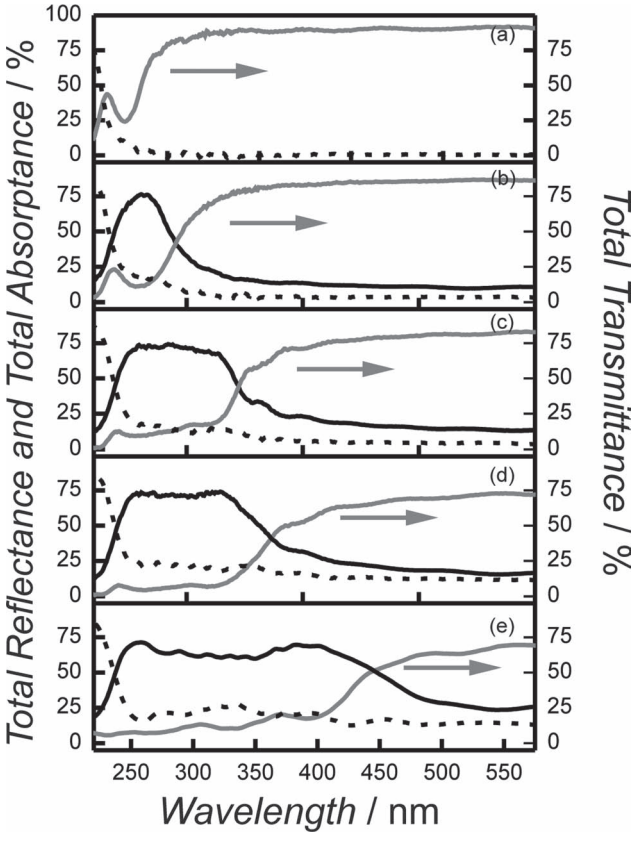

Figure 5. Total reflectance (black solid line), total transmittance (grey solid line) and absorptance (estimated as $1 - R_T - T_T$, black dotted line) spectra of different stacks of the flexible multilayer containing films shown in Figure 4a. The number of samples piled up is: a) 1, b) 2, c) 3, d) 5, and e) 7.

(AM1.5, 1000 W/m^2) during the same time. Films tested were: 1) a stack of multilayers that blocks the full UV region (sample ML_A); 2) another Bragg mirror pile that mimics the absorption profile of TiO_2 (sample ML_B); 3) a PDMS film containing a layer of TiO_2 nanoparticles with the same thickness than the photonic crystal (approximately 1 μm); 4) a PDMS film onto which a thin layer of benzophenone-3 was deposited; and 5) a PDMS film, to quantify the effect of receiving this amount of radiation without protection. In **Figure 6**a we show the energy per unit area received by the strips in each case. The corresponding transmittance spectra are plotted in Figure 6b. Remarkably the ability of the flexible interference mirror tandem ML_B to shield against UV rays is as good as that of a similar film of highly absorbing TiO_2 particles, while the performance of ML_A surpasses that of the film onto which benzophenone-3 was deposited. This shows that flexible photonic materials are suitable substitutes of inorganic or organic UV absorbers traditionally employed to dope polymers to the same end. The expected downshift of the spectral position of the reflectance peak for oblique angles of light incidence on multilayers, which follows a combination of Bragg and Snell laws, is in our case easily compensated by designing a stack of multilayers for which the longer cut-off wavelength is approximately 30 nm above the lower energy edge of the range to be blocked, since that is the peak shift measured at 45°. It should be noted that in order to make use of the protecting character of organic UV absorbers in a film, these compounds must be incorporated within the polymeric matrix, rather than deposited on top as it is done for the comparative study herein presented. Excited benzophenone is known to abstract hydrogen atoms from almost all polymers, thus generating radicals, which can be produced locally at high concentration and give rise to the degradation of the matrix.[43] Hence, one of the main advantages of integrating the nanostructured inorganic multilayers herein proposed is the absence of any

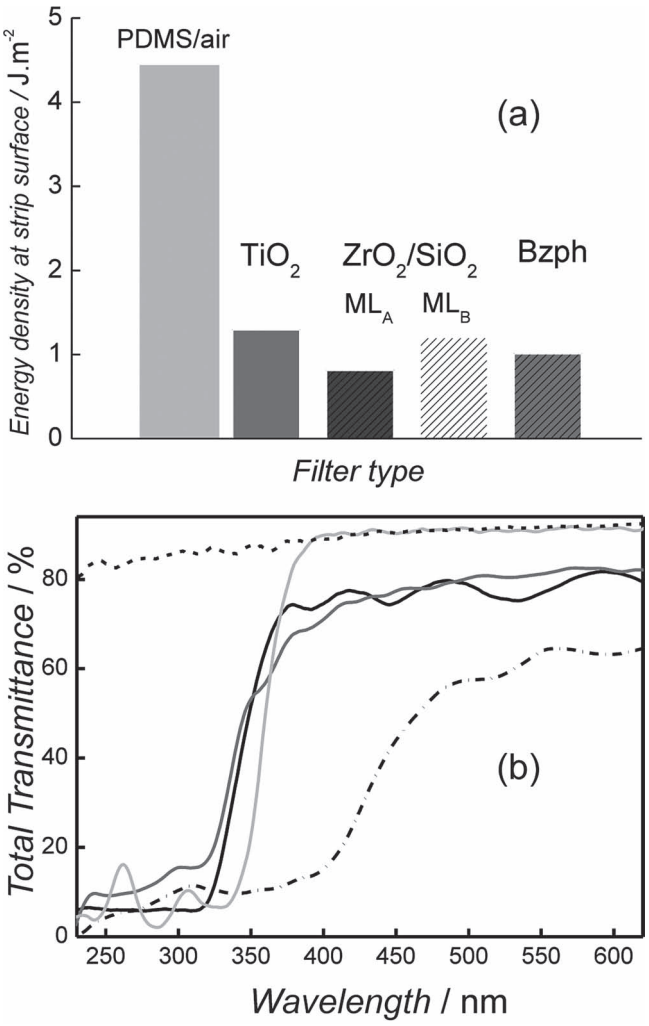

Figure 6. a) Energy density received at the surface of UV sensitive strips covered with different flexible UV protective films and exposed to a solar simulator (AM 1.5 spectrum, 100 mW/cm^2). Height of the bar represents the average value and the black line represents the standard deviation. ML_A and ML_B stands for different ZrO_2/SiO_2 film stacks. b) Total transmittance spectra of the protecting films used in Figure 6a: pure PDMS or naked strip (black short dashed line), TiO_2 nanoparticle film embedded in PDMS (black solid line), benzophenone-3 deposited (light gray solid line) onto PDMS, MLA (black dot dashed line), and MLB (gray solid line).

sort of photodegradation of the polymeric matrix without compromising the achievable degree of UV protection. Also, degradation of the polymer typically results in yellowing of the film, strongly reducing its transparency after some time.

3. Conclusions

We have shown a method to prepare both rigid coatings and flexible self-standing films capable of efficiently protecting against UV radiation in desired and preselected wavelength ranges. The UV blocking effect arises exclusively from optical interference phenomena and depends only on the number of stacked layers and the refractive index contrast between them. We demonstrate that these films may equal or outperform layers of similar thickness made of purely absorbing materials in terms of the degree of radiation protection achieved. These new materials offer a degree of protection comparable to that of traditional ones, but without any foreseeable unwanted secondary effects, such as photodegradation, increase of local temperature or, as it is the case for organic absorbers, generation of free radicals, all of them caused by light absorption.

4. Experimental Section

Preparation of Particle Suspensions: ZrO_2 nanoparticle sols were synthesized using a procedure based on the hydrolysis of zirconium n-propoxide.[35] A stable colloidal suspension of ZrO_2 nanoparticles was achieved by the slow addition of zirconium n-propoxide (3.7 mL, 70%, Alfa Aesar) in Milli-Q water (50 mL) acidified with HNO_3 (1 mL, 65%, Prolabo) under strong stirring. Immediately after the addition of the zirconium alkoxide a white precipitate is formed. The complete peptization of the solid took place under room temperature for approximately 72 h. Next, the colloidal suspension was dialyzed against pure Milli-Q water in a membrane (MWCO = 10 000, Spectra/Pore) until pH = 3.5. The final dialysis pH was the parameter employed to control aggregation and thus particle size distribution. Finally, water was removed by distillation at reduced pressure and particles were re-suspended in methanol. SiO_2 nanocolloids were purchased from Dupont (LUDOX TMA, Aldrich). Both suspensions were diluted in methanol in concentrations ranging from 3 to 4 wt% for ZrO_2 and from 1 to 4 wt% for SiO_2 particles.

Other methods involving the hydrolysis of zirconium alkoxide under the presence of tetralkylammonium salts in aqueous media did not lead to stable colloidal suspensions of ZrO_2 as poly-anion chains of Zr-O could not be broken by the ammonium salts. Steric repulsions due to the coordination of the alkyl chain to the oxide seemed to be insufficient to prevent aggregation. Commercial ZrO_2 suspensions were also tested without success.

Deposition of Nanoparticle-Based 1D Photonic Crystals: Photonic crystals were built by alternated deposition of ZrO_2 and SiO_2 nanoparticle suspensions, following a generic procedure previously reported.[31] Suspensions were deposited over quartz slides using a spin coater (Laurell WS-400E-6NPP), in which both the acceleration ramp and the final rotation speed could be precisely determined. Final speed was chosen between nominal value of 4500 and 6000 rpm and acceleration was set at 11 340 rpm s^{-1}. Suspensions were spun during 60 s. Sequentially, layers of different types of nanoparticles were deposited following the procedure described above. The process was repeated until the desired number of layers has been deposited.

Polymerization within the Multilayer Interstices and Lifting-Off: Elastomeric precursor and curing agent of PDMS (Sylgard 184, Dow Corning) was infiltrated depositing 0.5 g of the mix on top and then by spin coating (40 s, 700 rpm). After that, samples were maintained at room temperature during 24 h to facilitate the diffusion throughout the pore network. Next, PDMS was polymerized in a stove at 110 °C for 30 min. In order to lift off the flexible photonic structures, samples were immersed in liquid nitrogen (–196 °C). Then samples were allowed to warm up to temperature before being lifted off the substrate.

Optical and Structural Characterization: Total reflectance (R_T) and total transmittance spectra (T_T) were obtained using a UV-visible scanning spectrophotometer (SHIMADZU UV-2101PC) attached to an integrating sphere. Spectrophotometer slits were adjusted to measure R_T and T_T with the same spot size. Absorptance (A) was calculated from independent measurements of T_T and R_T by using $A = 1 - (R_T + T_T)$. Film images were acquired using a SLR digital camera (Pentax Kx). FESEM images of the multilayers films deposited onto silicon were taken by using a microscope Hitachi 5200 operating at 5 kV.

Solar Irradiation Experiments: Sample irradiation was carried out using a solar simulator (Sun 2000, Abet Technologies) including a 150 W xenon lamp with an appropriate filter for the correct simulation of the AM1.5 solar spectrum. A timer-controlled mechanism opened and closed the shutter. The incident light power was confirmed to be 1000 W/m^2 (1 sun) using a calibrated silicon solar cell. UV sensitive strips were purchased from UV process Supply Inc. (Control Cure, UV FastCheck Strips). Flexible films were placed on top of the sensitive strips and then the shutter was opened for 45 s. Both naked strips or PDMS film covered ones were used to determine the relationship between energy density received at the strip surface and the color change observed (see Supporting Information, Figure S5). These were quantified by measuring the total reflectance of the strips in an integrating sphere. In order to ensure the reproducibility of the protection effect, irradiation experiments were repeated three times and the results averaged.

Supporting Information

Supporting Information is available from the Wiley Online Library or from the author.

Acknowledgements

We thank the Spanish Ministry of Economy and Competitiveness for funding under grants MAT2011-23593 and CONSOLIDER HOPE CSD2007-00007, and Junta de Andalucía for grants FQM3579 and FQM5247. H.M. thanks the European Research Council for the Starting Grant POLIGHT.

Received: September 7, 2012
Revised: November 5, 2012
Published online: January 22, 2013

[1] Q. Ren, R. P. Gailitis, K. P. Thompson, J. T. Lin, *J. Quantum Electron.* **1990**, *26*, 2284.
[2] N. Serpone, D. Dondi, A. Albini, *Inorg. Chim. Acta* **2007**, *360*, 794.
[3] T. Bintsis, E. Litopoulou-Tzanetaki, R. K. Robinson, *J. Sci. Food Agric.* **2000**, *80*, 637.
[4] R. Lopez Cisneros, A. Gutarra Espinoza, M. I. Litter, *Chemosphere* **2002**, *48*, 393.
[5] M. Nowick, A. Richter, B. Wolf, H. Kaczmarek, *Polymer* **2003**, *44*, 6599.
[6] P. A. Rui Yang, T. A. Christensen, J. R. Egerton, E. White, *Polym. Degrad. Stab.* **2010**, *95*, 1533.
[7] A. L. Andrady, H. Hamid, A. Torikai, *Photochem. Photobiol. Sci.* **2011**, *10*, 292.
[8] R. P. Singh, N. S. Tomer, S. Veera Bhadraiah, *Polym. Degrad. Stab.* **2001**, *73*, 443.
[9] a) M. Norval, R. M. Lucas, A. P. Cullen, F. R. de Gruijl, J. Longstreth, Y. Takizawa, J. C. van der Leun, *Photochem. Photobiol. Sci.* **2011**, *10*, 199; b) K. Bolton, K. B. S. Martincigh, L. F. Salter, *J. Photochem. Photobiol.* **1992**, *63*, 241.
[10] W. W. Ting, *Int. J. Dermatol.* **2003**, *42*, 505.
[11] D. Brash, *Trends Genet.* **1997**, *13*, 410.
[12] C. A. Cole, J. Vollhardt, C. Mendrok, *Clinical Guide to Sunscreens and Photoprotection*, (Eds: H. W. Lim, Z. D. Draelos), Informa-Healthcare USA Inc., New York **2009**, pp. 39–51.
[13] M. Zayat, P. Garcia-Parejo, D. Levy, *Chem. Soc. Rev.* **2007**, *36*, 1270.
[14] M. M. Demir, K. Koynov, U. Akbey, C. Bubeck, I. Park, I. Lieberwirth, G. Wegner, *Macromolecules* **2007**, *40*, 1089.
[15] M. E. Calvo, J. R. Castro Smirnov, H. Miguez, *J. Polym. Sci. Part B: Polym. Phys.* **2012**, *50*, 945.
[16] G. S. Liou, P. H. Lin, H. J. Yen, Y. Y. Yu, T. W. Tsai, W. C. Chen, *J. Mater. Chem.* **2010**, *20*, 531.
[17] Y. Tu, L. Zhou, Y. Z. Jin, C. Gao, Z. Z. Ye, Y. F. Yang, Q. L. Wang, *J. Mater. Chem.* **2010**, *20*, 1594.
[18] L. Mazzocchetti, E. Cortecchia, M. Scandola, *ACS Appl. Mater. Interfaces* **2009**, *1*, 726.
[19] D. Koziej, F. Fischer, N. Kränzlin, W. R. Caseri, M. Niederberger, *ACS Appl. Mater. Interfaces* **2009**, *1*, 1097.
[20] A. Macleod, *Thin film optical filters, 3rd ed.*, Institute of Physics Publishing, London **2001**.
[21] J. D. Joannopoulos, S. G. Johnson, J. N. Winn, R. D. Meade, *Photonic crystals: molding the flow of light, 2nd ed.*, Princeton University Press, Princeton **2008**
[22] M. Abid, T. Moudakir, G. Orsal, S. Gautier, A. En Naciri, Z. Djebbour, J.-H. Ryou, G. Patriarche, L. Largeau, H. J. Kim, Z. Lochner, K. Pantzas, 1 D. Alamarguy, F. Jomard, R. D. Dupuis, J.-P. Salvestrini, P. L. Voss, A. Ougazzaden, *Appl. Phys. Lett.* **2012**, *100*, 051101.
[23] S. F. Chichibu, T. Ohmori, N. Shibata, T. Koyama, *Appl. Phys. Lett.* **2006**, *88*, 161914.
[24] T. K. Kim, S. S. Yang, J. K. Son, Y. G. Hong, G. M. Yang, *Appl. Phys. Lett.* **2006**, *89*, 041129.
[25] D. J. Schroeder, *J. Opt. Soc. Am.* **1962**, *52*, 1380.
[26] B. Bates, D. J. Bradley, *Appl. Opt.* **1966**, *5*, 971.
[27] E. Spiller, *Appl. Opt.* **1976**, *15*, 2333.
[28] A. Urbas, R. Sharp, Y. Fink, E. L. Thomas, M. Xenidou, L. J. Fetters, *Adv. Mater.* **2000**, *12*, 812.
[29] J. Bailey, J. S. Sharp, *J. Polym. Sci., Part B: Polym. Phys.* **2011**, *49*, 732.
[30] P. Zavala-Rivera, K. Channon, V. Nguyen, E. Sivaniah, D. Kabra, R. H. Friend, S. K. Nataraj, S. A. Al-Muhtaseb, A. Hexemer, M. E. Calvo, H. Miguez, *Nat. Mater* **2012**, *11*, 53.
[31] S. Colodrero, M. Ocaña, H. Míguez, *Langmuir* **2008**, *24*, 4430.
[32] M. E. Calvo, S. Colodrero, N. Hidalgo, G. Lozano, C. López, O. Sánchez-Sobrado, H. Míguez, *Energy Environ. Sci.* **2011**, *4*, 4800.
[33] M. E. Calvo, O. Sánchez-Sobrado, G. Lozano, H. Míguez, *J. Mater. Chem.* **2009**, *19*, 3144.
[34] M. E. Calvo, H. Miguez, *Chem. Mater.* **2010**, *22*, 3909.
[35] Q. Xu, M. A. Anderson, *J. Mater. Res.* **1991**, *6*, 1073.
[36] a) Z. Wu, D. Lee, M. F. Rubner, R. E. Cohen, *Small* **2007**, **3**, 1445; b) L. D. Bonifacio, B. V. Lotsch, D. P. Puzzo, F. Scotognella, G. A. Ozin, *Adv. Mater.* **2009**, **21**, 1641.
[37] J. H. Prosser, T. Brugarolas, S. Lee, A. J. Nolte, D. Lee, *Nano Lett.* **2012**, *12*, 5287.
[38] F. Gallego-Gómez, V. Morales-Flórez, A. Blanco, N. de la Rosa-Fox, C. López, *Nano Lett.* **2012**, *12*, 4920.
[39] O. Sánchez-Sobrado, G. Lozano, M. E. Calvo, A. Sánchez-Iglesias, L. M. Liz-Marzán, H. Míguez, *Adv. Mater.* **2011**, *23*, 2108.
[40] G. Lozano, S. Colodrero, O. Caulier, M. E. Calvo, H. Míguez, *J. Phys. Chem. C* **2010**, *114*, 3681.
[41] J. A. Parrish, K. F. Jaenecke, *J. Invest. Dermatol.* **1981**, *76*, 359.
[42] L. Scherschung, J. J. Kim, H. W. Lim, *J. Am. Acad. Dermatol.* **2001**, *44*, 999.
[43] M. H. Schneider, Y. Tran, P. Tabeling, *Langmuir* **2011**, *27*, 1232.